# Failure Mechanism and Seismic Performance Evaluation of Steel Frame using Rocking Truss

Mingming Jia[1, 2], Shan Gao[1*, 3], Feng Fu[4] and Ning Yang[1]

[1] School of Civil Engineering, Harbin Institute of Technology, Harbin 150090, China

[2] Key Laboratory of Earthquake Engineering and Engineering Vibration, Institute of Engineering Mechanics, China Earthquake Administration, Harbin 150080, China

[3] Postdoctoral Station of Civil Engineering, Chongqing University, Chongqing 400000, China

[4] School of Mathematics, Computer Science and Engineering, City, University of London, London EC1V0HB, UK

**Abstract.** To mitigate the deficiency of the conventional steel frames, a novel steel frame system using rocking truss (SFWRT) and self-centering energy dissipative devices (SCED) was developed. The SCED consists of structural members, pre-tension tendons, abutting element and friction dissipation devices, which exhibits excellent self-centering and energy dissipation capacity. This new structural system is analyzed using Incremental Dynamic Analysis method (IDA). A scaled earthquake acceleration response spectrum from a specified ground motion was used in this analysis. It is found that the formation of the plastic hinges of the structural components includes four stages: emergence, developing, degradation and completely bearing capacity loss. A comparative study is also made to investigate the development of these plastic hinges under different ground motions in both traditional steel frame and SFWRT. The results for evaluating the lateral collapse resistance capacity indicate that the rocking truss can significantly decrease the structural dynamic response and improve the seismic performance of buildings. The collapse probability curves of the steel frame and SFWRT based on three limit states are compared. It is found that the rocking truss is helpful to reduce the collapse probability under earthquakes. The damage of the steel frame as well as the expected loss of the main structure after an earthquake can be significantly reduced with the help of rocking truss, which would also reduce the repair cost and improve the structural resilience under earthquakes significantly.

**Keywords:** rocking truss; incremental dynamic analysis; failure modes; seismic performance; collapse probability

## 1. Introduction

Conventional structural systems to resist earthquake include moment-resisting frames (MRFs), dual frame-walls, and dual frame-braces. The inelastic deformations of primary structural members are adopted to dissipate seismic energy and protect structures against collapse, which always causes unacceptable residual deformation and unexpected failure modes (Eatherton et al. 2008, Matthew et al. 2014). The performance-based earthquake engineering (PBEE) also emphasizes on reducing seismic damage in the design. It is imperative to investigate on effective way to improve the structural performance under earthquake. In general, higher seismic performance can be achieved by minimizing inelastic deformation and damage to primary structural components and residual drifts. Thus, in this paper, a series of new approaches were developed to enhance the performance of the structure under earthquake. A new type of rocking truss-steel frame is developed here as a low-damage structural system, which can improve the performance of the structure, limit the area of the damage in replaceable structural members and eliminate residual drifts.

Particularly, the rocking of structures has been investigated for a long time, Clough and Huckleridge (1977) performed the earliest shaking table tests on rocking steel frames, which demonstrated potential benefits of rocking. Then a number of experimental and numerical researches were conducted. Midorikawa et al. (2002, 2014) added baffle plate to the column bases of rocking structures to allow the column uplifted under earthquakes, and the results showed that the bucking of the plate could significantly dissipate energy. Gunay et al. (2009) evaluated that the use of rocking concrete walls can form a rigid core to attract seismic forces and limit demands on non-ductile framing, which potentially prevented soft story from failures. Qu et al. (2009, 2010, 2011) further advanced the design theory of rocking concrete walls through a practical engineering. However, once the rocking concrete wall is damaged, it is difficult to repair in time and the cost may be relatively high. On the other hand, other researchers (Tremblay et al. 2008, Deierlein et al. 2011) have explored the installation of dampers at the column bases to reduce the structural seismic response. There were some different typical frames and components (MacRae et al. 2004, Wu 2013, Du et al. 2014, Pollino et al. 2013, Chirstopoulos et al. 2008) (such as rocking truss and self-centering energy dissipative devices), which were also useful for mitigating the damage and providing sufficiently self-centering capacity.

The rocking buckling-restrained brace frame (RBRBF), allowing the column base uplifting during strong earthquakes, which decreases seismic damage and reduce repair cost after seismic event. The liftable column bases with friction dampers could improve the energy absorption capacity of the rocking structure model (Zhang et al. 2018). Dar et al. (2018) introduced a rocking block model that was dynamically equivalent to a rocking frame with vertically symmetric piers of any geometry. A new finite element model to analyze the seismic response of deformable rocking bodies and rocking structures had been presented whose results showed that a deformable rocking frame was more stable than its rigid counterpart (Vassiliou et al.

*Corresponding author, GAO Shan, Associate Professor, E-mail: 13833185232@139.com

2017). Kibriya et al. (2018) proposed a finite element model of steel building to enable an accurate representation of the complex nonlinear dynamics of self-centering structures, over a wide range of excitation frequencies and amplitudes, and captures the appearance of sub-harmonic resonances and higher-modes. Blebo et al. (2018) developed a pin-supported self-centering rocking core system with buckling-restrained columns (SCRC-BRC) to provide significant drift capacity while limiting damage due to residual drift and soft-story mechanisms. Kamperidis et al. (2018) proposed a partial-strength low-damage self-centering steel column base, which provided flexibility in the design. Jia et al. (2018) conducted a time history investigation on a newly proposed type of self-centering dual-steel buckling-restrained braces (SC-DBRBs) whose results showed that the SC-DBRB could effectively reduce residual drift. Keivan and Zhang (2019) conducted a study of a Y-type self-centering eccentrically braced frame (SCEBF-Y). The nonlinear time history analysis results revealed that not only the SCEBF-Y structure had negligible residual drift, but also major damage concentrates on replaceable energy dissipation devices.

Considering the widely used rocking braced steel frames (Gledhill et al. 2008, Hall and Eatherton 2010, Michael 2015), the advantages of the rocking truss and the self-centering devices are combined together and a self-centering rocking truss-steel frame system was introduced in this research. Finite element models were established in OpenSEES to study the failure modes and structural performance of the steel frame (SF) and steel frame with rocking truss (SFWRT). Due to the various structural response of this type of structure, a novel probabilistic damage evolution analysis method and the fragility analysis of the prototype structure were performed to achieve the optimization and control of the failure modes of the steel frames.

## 2. FE analysis of prototype structures

### *2.1 Structural System Modelling*

Two eight-story prototype structures including one conventional steel frame and one steel frame with self-centering rocking truss (SFWRT) are designed as shown in Figure 1. It is assumed that the structure is located on firm rock (site Class II in GB50011-2010 (2010)). The site has the fortification earthquake intensity of VIII degree, which has a corresponding design characteristic period of 0.4s, with the design fundamental acceleration of 0.2g (g is the gravity acceleration). It is worth mentioning that 4 typical loads are considered in this structure, the dead load and live load at each story are considered as 3.0kN/m$^2$ and 2.0kN/m$^2$, respectively. Simultaneously, the basic wind load is chosen as 0.45kN/m$^2$, and the basic snow load is 0.25kN/m$^2$. More detail information about columns, beams and other geometrical configurations of the steel frame structure are listed in Table 1. It should be mentioned that the floor is not modeled and only the dead load of the floor is considered in the model. The design of Self-Centering Energy Dissipative device (SCED) was presented in section 2.2.

Finite element (FE) models of the steel frame (SF) and steel frame with self-centering rocking truss (SFWRT) were built in the OpenSEES. The nonlinear-Beam-Column element was used to simulate the beam, column members with considering the second-order effect (P-$\Delta$ effect), and the corresponding hysteresis constitutive model of the materials were chosen as shown in Figure 2. The degradation of strength and stiffness of steel material are considered in this model. In the backbone curve, $K_e$ is the elastic stiffness, $F_y$ is the yielding strength, the strain hardening stiffness is $K_s=\alpha_s K_e$, the deformation at peak point is $\delta_c$ and the yielding deformation is $\delta_y$, $\delta_c/\delta_y$ is the ductility of steel. After reaching the peak point, the strength and stiffness of steel begin to degrade due to the steel necking effect. The degraded stiffness is $K_c=\alpha_c K_e$ and residual strength is $F_r=\lambda F_y$. The parameters of the hysteresis constitutive model of steel are listed in Table 2.

Since there is no corresponding tested specimen to validate the model, the first natural period of the building from the analysis is compared with that calculated by the empirical formula (1) and derived from the equation (2) (as listed in Tab.3). The formula (1) is defined according to Chinese building code (2010). The equation (2) is recommended by Chopra and Goel (2014). The dispersion of the results is very little, so the FE model in OpenSEES was calibrated based on structural natural periods and structural responses. It was found that a FE model in OpenSEES can be calibrated to give a good prediction of earthquake response, since the earthquake response of multi-storey regular building mainly depends on its fundamental natural period. Other modeling techniques including material property model, element and interaction property have also been validated against the SAC steel project models in terms of maximum displacement, story drift angle, story speed story acceleration and base shear. More details can be found in Jia et al (2019).

$$T_1 = (0.10\text{-}0.15)n \tag{1}$$

$$T_L = (0.016 - 0.023)H^{0.9} \tag{2}$$

Where $n$ is the total number of floors in the building, $H$ is the total height of the building in feet.

Table 1 The detail information of the steel frame

| Story | Story height (mm) | Column section | Beam section | Truss section | Thickness of the floor(mm) |
|---|---|---|---|---|---|
| 1F | 3900 | HW350×350×12×19 | HW250×250×9×14 | □200×5 | 100 |
| 2F | 3300 | HW350×350×12×19 | HW250×250×9×14 | □200×5 | 100 |

| | | | | | |
|---|---|---|---|---|---|
| 3F-5F | 3300 | HW344×348×10×16 | HW250×250×9×14 | □200×5 | 100 |
| 6F-8F | 3300 | HW300×300×10×15 | HW250×250×9×14 | □200×5 | 100 |

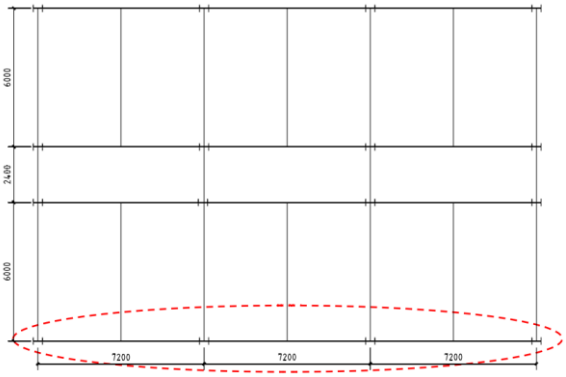


(a) Plane layout

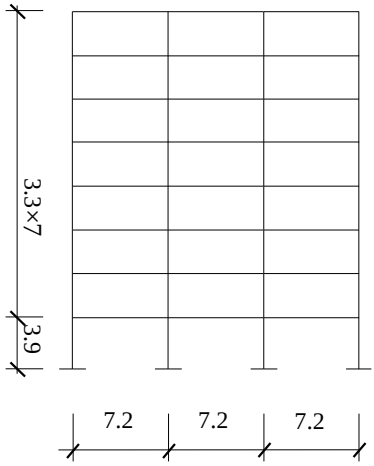


(b) Conventional frame

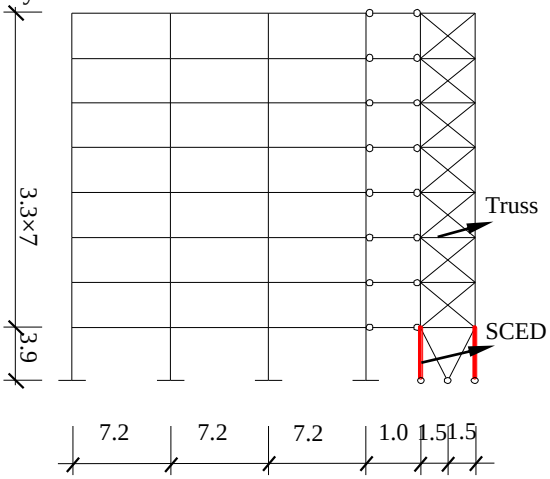


(c) Frame with SFWRT

Fig. 1 The elevation configuration for the example structures (m)

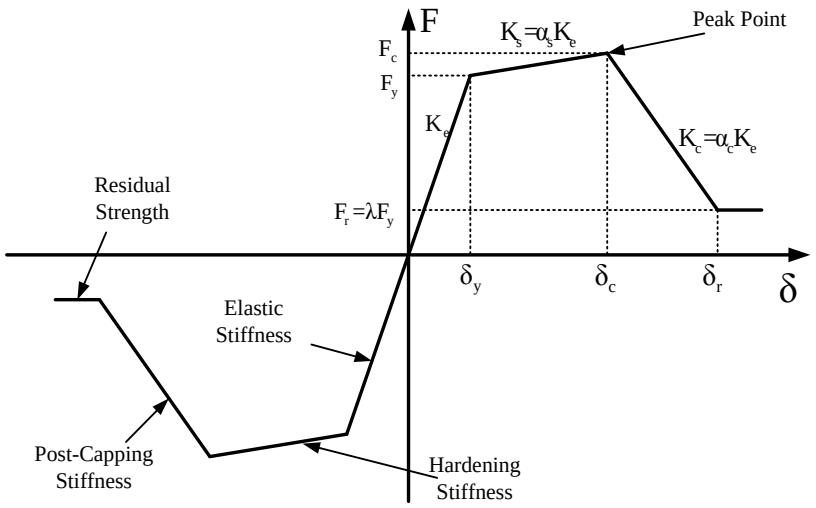


Fig. 2 The hysteretic constitutive model of steel: backbone curve

Table 2 Parameters of the hysteresis constitutive model of steel

| Steel | $K_e$ ( MPa ) | $F_y$ ( MPa ) | $\alpha_s$ | $\delta_c/\delta_y$ | $\alpha_c$ | $\lambda$ |
|---|---|---|---|---|---|---|
| Q235 | 200,000 | 235 | 0.02 | 18 | -0.02 | 0.2 |

Table 3 Comparison of the first natural periods (s)

| Method | OpenSEES | Chinese codes | Chopra |
|---|---|---|---|
| natural period | 0.950 | (0.80-1.20) | (0.90-1.26) |

### *2.2 Finite element modelling and verification of SCED*

The Self-Centering Energy Dissipative device (SCED) in Christopoulos et al. 2008 consists of structural members, pre-tension tendons, abutting element and friction energy dissipation devices. A series of simulations were performed in advance to determine the geometrical and physical properties of the SCED. In this paper, the outer square tube size is designed as HSS305×305×8mm with cross section of 9504mm$^2$; the inner square tube size is HSS254×254×8mm with cross section of 7872mm$^2$. Four Technora-T200 fiber cables with diameter 17mm are adopted as pre-tension tendons, and the friction force and per-tension are set as 276kN, 280kN respectively, and the total length of the member is 2170mm. The loading rule curve in the test is shown in Table 4.

The rocking truss and SCED are simulated by the Truss element and Two Node Link element which is defined by two nodes as shown in Fig. 3, respectively. Besides 6 degrees of freedom, if this Two Node Link element length is larger than zero, the P-Delta moments around the local x and y axis can be specified. In other words, the specific configuration of the SCED is not considered in the modeling. The constitutive relation of the Self-Centering was selected in the SCED simulation. The comparison between the test results and the numerical simulation is shown in Figure 4 below, which indicates that the hysteresis curves obtained from the OpenSEES are basically consistent with the experimental data in terms of stiffness and bearing capacity, and the SCED braces can be well simulated by the Two Node Link element and the Self-Centering constitutive relationship defined in OpenSEES. The experimental data shows that the stiffness and strength of the SCED bracing system slightly degrade in the unloading stage. However, since the damage accumulation and unloading stiffness degradation are not taken into account in the current OpenSEES, the differences can be seen in Figure 4. In general, the FE model is accurate enough to meet the need of further research.

Table 4 Loading system curve (mm)

| Number of cycles and their corresponding magnitude | | | | | | | | | | | | |
|---|---|---|---|---|---|---|---|---|---|---|---|---|
| 1 | 2 | 3 | 4 | 5 | 6 | 7 | 8 | 9 | 10 | 11 | 12 | 13 |
| 2.17 | 4.34 | 6.51 | 8.68 | 10.85 | 13.02 | 15.19 | 17.36 | 19.53 | 21.7 | 23.87 | 26.04 | 28.21 |

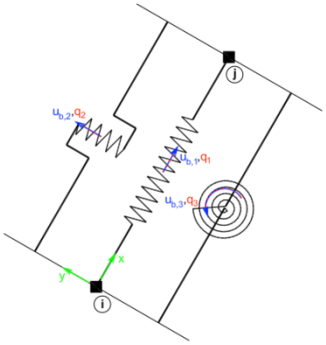

Fig. 3 Two node link element

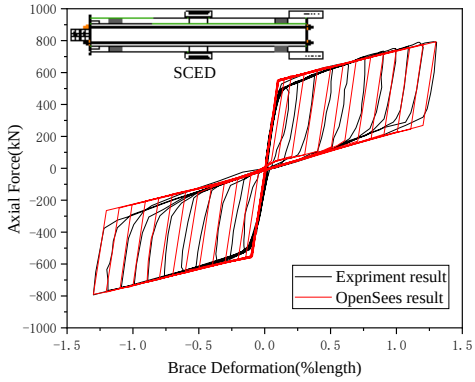


Fig. 4 Comparison of SCED component test and numerical simulation results (Christopoulos et al. 2008)

### *2.3 The Selection of Ground Motions*

Based on FEMA P695 (2009), 22 strong far-field ground motions (with relative higher peak ground velocity) named from GM1 to GM22 respectively were selected for seismic analysis. The ground motions are selected based on their suitability for the collapse assessment of structures. The corresponding earthquake acceleration response spectrum and median response spectrum at the first-mode period are shown in Figure 5.

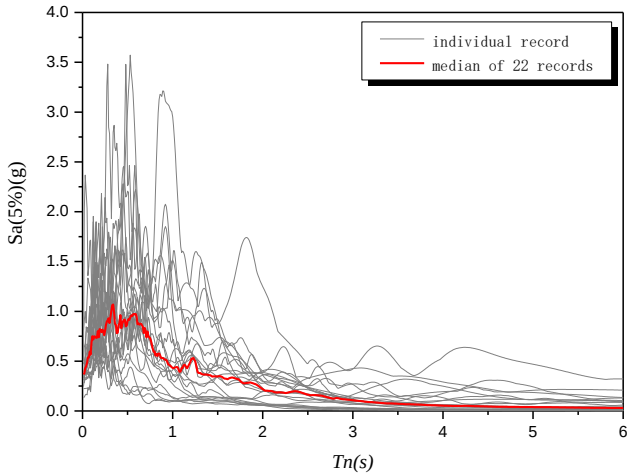


Fig. 5 Earthquake acceleration response spectrum and median response spectrum of 22 ground motions

## 3. Evolution of structural damage

For a specific ground motion, the scaled acceleration response spectrum is adopted to analyze structural responses until the structure collapses. The development of plastic hinges followed four stages: emergence, developing, degradation and completely bearing capacity loss. Especially, a plastic hinge is assumed to occur when the yielding is observed in the flexural members. There is variability/uncertainty among different earthquake records (Record-to-Record variability), which causes the different developing sequences and amounts of plastic hinges, but there are some similarities of the component failure sequences and the failure mode among the structures. Therefore, it is necessary to make statistical analysis of the structural plastic hinges' formation sequence and structural failure mode to reveal the failure mechanism.

### *3.1 The formation sequences of the plastic hinges*

Statistical analysis of the formation sequences of plastic hinges under different ground motions are made, and the mean value of sequence number of the same structural member is adopted to depict the development of plastic hinges. Meanwhile, the mean values of sequence numbers are normalized into the value range of (0, 1) for comparing the formation process of plastic hinges between SF and SFWRT. If the normalized sequence number value closes to 0, it indicates that the member yields earlier. In contrast, a larger value indicates the member yielding later, in other words, less ductility performance under earthquake.

The dispersion of the plastic hinges developing sequence is also important to quantify the uncertainty of structural failure modes, so the standard deviations of sequence numbers are also calculated and denoted in Figure 6. A smaller standard deviation indicates the occurrence of the plastic hinges has less uncertainty, which also indicates the damage evolution during an earthquake can be predicted more accurately. Thus, the approximate failure path and plastic hinge development patterns are obtained.

It can be seen from the Figure 6 and 7 that the differences of plastic hinges formation and development between SF and SFWRT are large, and the plastic zones develop earlier at the columns of the SF. What's more, the plastic hinges of the column ends and the beam ends develop homogeneously, and some components remain elastic and fail to dissipate energy effectively, that is to say, the anti-seismic potential are not utilized adequately. The formation of plastic hinges in the columns are more or less later than the formation of plastic hinges in the beam ends of the SFWRT, which is beneficial to the energy dissipation and structural safety. In addition, the plastic hinges at the columns and beam ends develop more uniformly when using the rocking frame truss, and most of structural components participate in energy dissipation, so the seismic potential of structural system is realized well.

### *3.2 Failure modes analysis*

The detail information of the failure modes and corresponding earthquake intensities for the structure under different ground motions are summarized. As shown in Figure 8, the main failure modes for the SF can be classified to 4 types: the multi-stories failure of 1-4 stories, 1-6 stories, 1-3 stories and the single bottom story failure, and the corresponding failure probabilities are about 36.4%, 31.8%, 27.3% and 4.5%, respectively. Under the same intensity earthquake, the multi-stories failure mode is not observed for the SFWRT. The statistical results show that the collapse resistant capability of the SFWRT is apparently higher than that of the SF.

### *3.3 Comparative analysis of the formation sequence of plastic hinges*

In order to study the failure paths of steel frame and steel frame with rocking truss, a comparative study of the formation sequence of plastic hinges under ground motion GM19 is represented in Figure 9.

As can be seen from Figure 9 above, the failure sequence of the steel frame and the steel frame with rocking truss has the following different characteristics:

(1) The steel frame first yields at the bottom beam end, while the steel frame with rocking truss first yields at the foot of the middle column at which a plastic hinge is formed.

(2) The failure of the steel frame propagate from the middle beam end (2nd and 3rd story) to the bottom beam end (1st floor), and to the middle and high part beam end (4th, 5th, 6th story) and to the column base and finally to a variable system, Besides, plastic hinges tend to develop from the outer span to the inner span. Correspondingly, the failure mode of rocking truss is that the plasticity forms from the bottom to the top story for the entire building, and the plastic hinge is gradually formed from the outer span to the inner span.

(3) The failure path of the steel frame is short, and the member of top story does not yield. When the structure fails, the member of the top story maintains elastic and the utilization rate of the material is too low, and the damage is concentrated on the local part of structure, which results in low bearing capacity and ductility. However, when the steel frame with rocking truss fails, the structural plasticity develops more evenly, and no soft story developed, so the structural bearing capacity and ductility are improved.

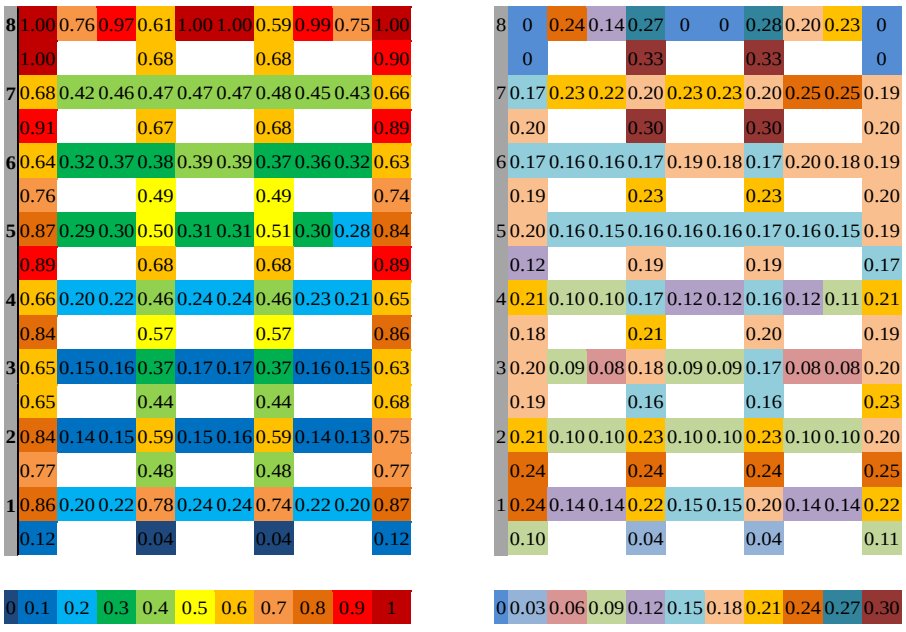


(a) The mean value of the developing sequence (b) The standard deviation of the developing sequence

Fig. 6 Statistic of the developing sequence of plastic hinges of SF

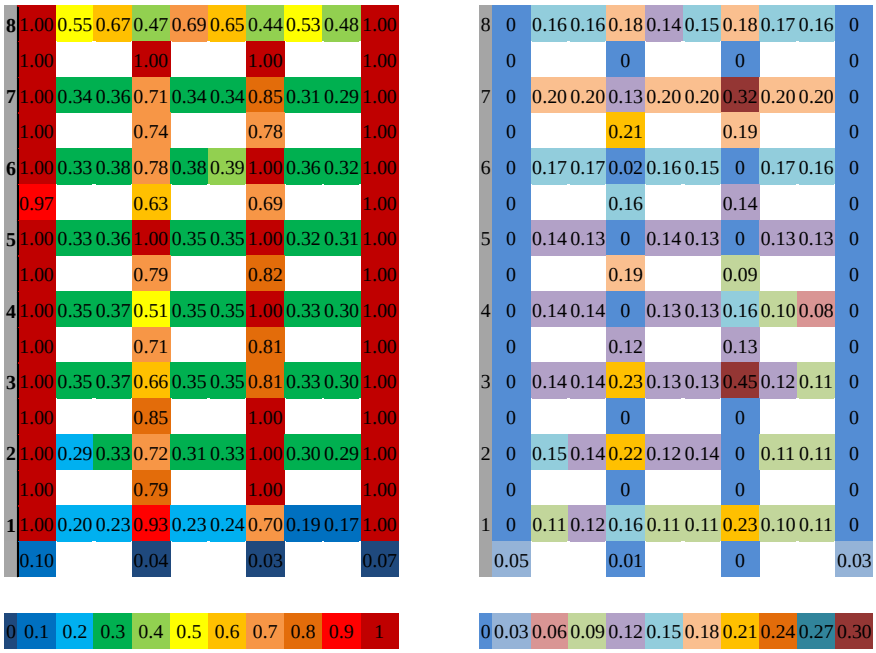


(a) The mean value of the developing sequence (b) The standard deviation of the developing

Fig. 7 Statistic of the developing sequence of plastic hinges of SFWRT

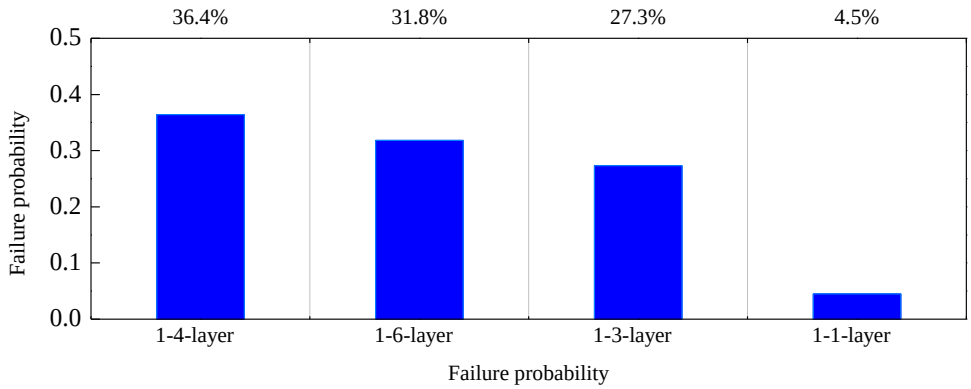


Fig. 8 The probabilities of different collapse failure modes of the SF

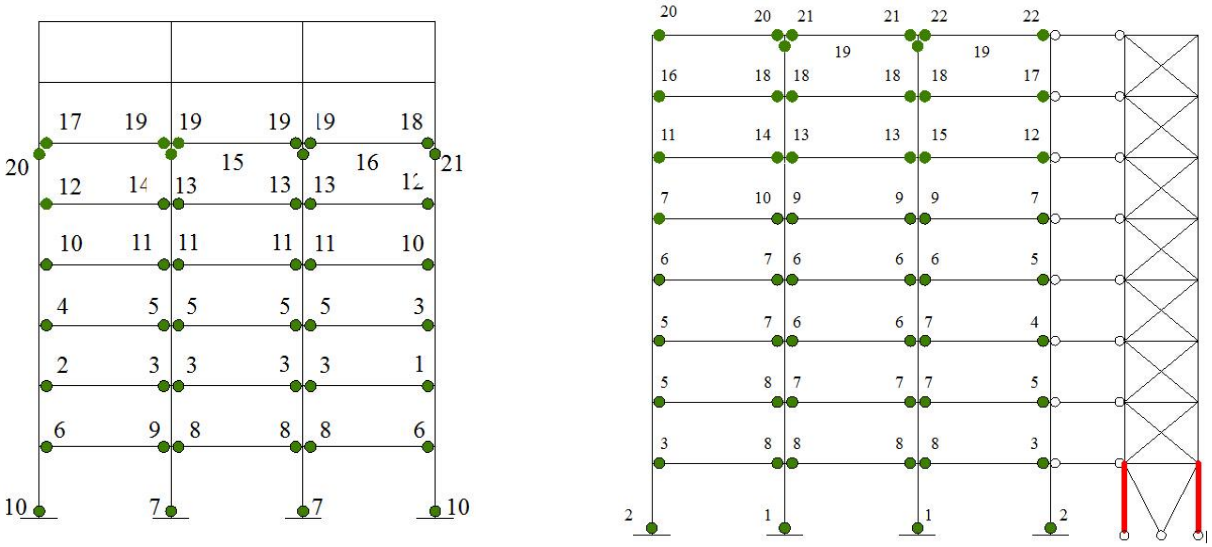

(a) The developing sequence of plastic hinges in steel frame

(b) The developing sequence of plastic hinges in steel frame with rocking truss

Fig. 9 Comparison of failure paths between steel frame structure and rocking truss-steel frame system under the earthquake record of GM19

## 4. Analysis of damage evolution of structural system

The steel frame studied in this paper adopts H-shaped steel section components. In the OpenSEES simulation, the failure criterion of components is determined by the fracture of the cross-sectional edge fiber in a beam element, and the bearing capacity of the components decreases instantly while components fail. The ductile Damage Index can be used to demonstrate the damage states of structural components conveniently, and a simple damage index corresponding to ductility ratio is proposed, which is calculated as follows:

$$DI = \frac{\delta_c}{\delta_u} = \frac{\delta_c / \delta_y}{\delta_u / \delta_y} = \frac{\mu}{\mu_u} \tag{3}$$

Where $\delta_c$ and $\delta_y$ represent the maximum deformation and yield deformation of the components, respectively, and $\delta_u$ represents the maximum deformation and maximum ductility of the components, respectively.

The outermost strain value is used to judge the damage state of the structural component. For the deformation value, when $\delta_c > \delta_y$, the member began to form plasticity; when $\delta_y < \delta_c < \delta_u$, the member is in strain hardening stage, and the corresponding DI < 1; when $\delta_c > \delta_u$, the member is in the degenerated stage after reaching the peak load bearing, and the corresponding DI > 1 at this time.

The process of plastic hinge developing and the damage evolution of structural components are related to the relationship of force and deformation of members. As shown in Figure 10, the damage statuses can be estimated according to the deformation amplitude, until the structure finally failed and collapsed.

The ratios of the inner circle radiuses to the outer circle radiuses indicate the different damage states of the components. When the structural component remains elastic, as shown in the first circle in Figure 10, the radius of the inner circle is extremely small, which is not shown in the structural damage evolution figure. As the structural component yields, the inner circle radius gets large to show the yielding state. When the load bearing capacity of the component reaches the ultimate, the damage state is represented by a solid blue circle. In the degradation stage of load bearing capacity of the component, the inner circle radius increases to be larger than the outer circle radius, and it is marked in red. Accordingly, the damage evolution diagrams of the structures are shown in Figure 11.

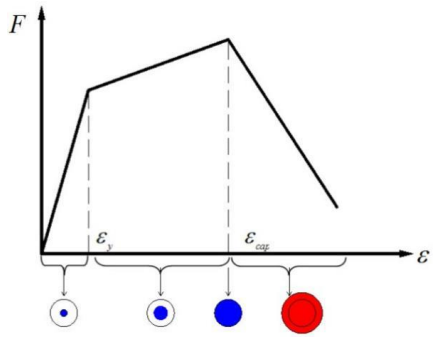


Fig. 10 Schematic diagram of structural plastic hinge developing and damage evolution

As it can be seen from Figure 11 above, the steel frame evolved from elasticity to plasticity under the action of GM1 ground motion, and the plastic hinges gradually developed and propagated in the structure. When Sa(T1,5%) = 1.1g, the large damage occurred on the column bottom of the first story and the column top of the fourth story of the steel frame, and the strength of corresponding components began to degenerate, which leads to the multi-stories failure mode from the first story to the fourth story, and then the global strength of the steel frame degenerates as the plastic hinges formation at the top of the 3rd story column and the 7th story column. When the damage accumulates at the end of beam, the constraint effect of beams on the column top ends is weakened, and the columns tend to increase rotation deformation. Therefore, the structure experienced large shear deformation, and the steel frame collapses ultimately due to excessive deformation. However, under the same magnitude of earthquake ground motion, the damage of steel frame with rocking truss is less than that of steel frame, and the damage of steel frame with rocking truss is mainly concentrated at the end of beam. With the exception of plastic hinges on the top end of both columns 2 and 3 in the 8th story, the columns of steel frame with rocking truss remain elastic, which is an ideal uniform damage condition. Thus, the rocking truss has a unique advantage in controlling the damage distribution of steel frames.

It is shown in Figure 12 that the damage evolution process of steel frame structure and steel frame with rocking truss under ground motion GM2. The plastic hinge developed from the ends of the beams to the ends of the columns, it can be seen that the inner columns yielded earlier and more plastic hinges formed in the inner columns. When the spectral acceleration is adjusted to *S*a(T1,5%) = 2.3g, not only the bottom of the steel frame is in the serious damage status, but also a large number of plastic hinges form at the end of the columns which resulted in the strength and stiffness degradation.

The bottom story is prone to lateral shear displacement under earthquake ground motion, and the performance degradation of the bottom stories leads to the multi-stories failure mode from the first story to the fourth story. With the addition of rocking truss, the damage reduction of the structure is concentrated in the ends of the beams, and structural damage is more uniform. The steel frame is more flexible and robust, and the structural energy dissipation ability is stronger. When the spectral acceleration is adjusted to *S*a (T1, 5%) = 2.3g, the plastic hinges with large damage are only at the ends of the beams and the bottom columns of main steel frame. Compared with the steel frame, the main structural columns have little damage. The collapse resistance capacity of the structure is also obviously improved.

## 5. Structural seismic performance evaluation

The peak displacements and relative angular story drift angles of a building under earthquake loading reflect the damage level of the structure. The residual displacements of the structures after earthquake usually are used to determine whether the structures can be used immediately or need to be repaired, which affects the potential economic cost of repair. Seismic performance and self-centering capacity are evaluated by the story angular drift and residual displacements of the structural systems, respectively.

### *5.1 Structural damage assessment*

According to different seismic intensities, the selected 22 earthquake records were further scaled based on fundamental period for elastoplastic time-history analysis. Wen and Kang (2009) studied the damage of the steel frame and obtained the relationship between the performance of the steel frame and the story drift ratio, which is listed in Table 5. The limits of each performance level of the steel frame are marked by thick blue lines in Figure 13.

In the case of frequent earthquakes, as shown in Figure 13a), the average drift ratio of the original steel frame is below 0.2% (Performance Level I). Based on the measured data, the structural responses are also depicted as mean $\mu$ plus standard deviation$\sigma$ ($\mu+\sigma$) for considering the dispersion of the ground motion records. The analysis results show that the drift ratio ($\mu+\sigma$) of steel frame is above 0.2% (in slight damage state), while the drift ratio ($\mu$,$\mu+\sigma$) of the steel frame with the rocking truss is below 0.2% (in no damage state).

In the case of fortification earthquakes, as shown in Figure 13b), according to the structural mean response, the original steel frame is yet at the performance level III. Due to the contribution of rocking truss, the structural performance level can be improved to the level II. Based on the $\mu+\sigma$ curves, the structural damage state is improved from Moderate to Light when it is in parallel with the rocking truss. The story deformation of the structure tends to be uniform, and there is no soft story in the system.

In the case of rare earthquake, as shown in Figure 13c), according to the structural mean response, the original steel frame system has reached the state of moderate damage, while the performance level of steel frame system with rocking truss is still in the light damage state. According to the $\mu+\sigma$ curves, although the two systems are in the same performance level, and the maximal drift ratio is decreased from 0.14 to 0.1 with the function of the rocking truss.

Meanwhile, it can be concluded from Figure 13 that the third story of the steel frame is a soft story under three earthquake intensities, and the story drift ratio of the third story is the largest as well. When the steel frame is installed with the rocking truss, the third story drift ratio of the structural system is dramatically declined, as shown in Table 6. Therefore, the rocking truss can significantly reduce the deformation of the original steel frame. The occurrence possibility of the soft story can be reduced and the damage distribution of the original steel frame is more even when the steel frame is installed with rocking truss, and most of the structural components take part in seismic energy dissipation, thereby the structural responses can be reduced.

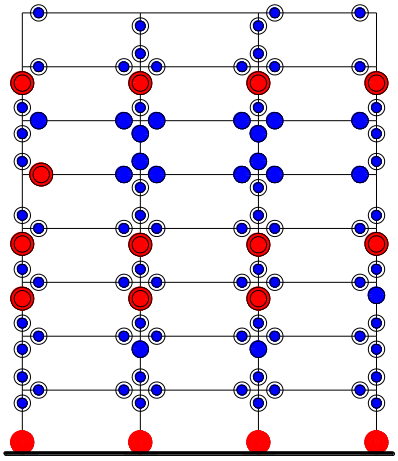

(a) damage diagram of steel frame at *S*a= 1.1g

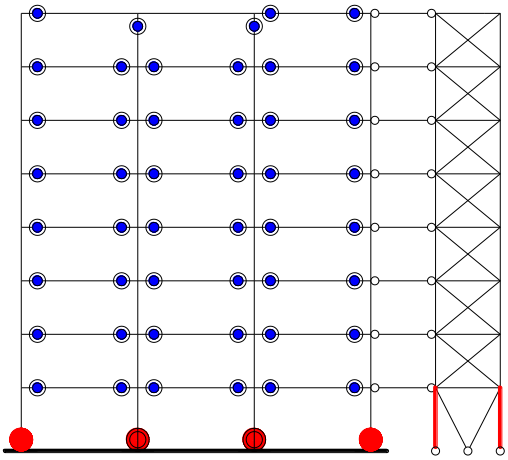

(b) damage diagram of rocking truss-steel frame at *S*a= 1.1g

Fig.11 The damage evolution process of steel frame structure and steel frame with rocking truss subjected to earthquake

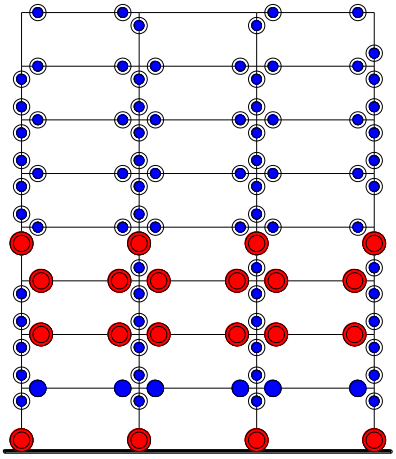

(a) The damage diagram of steel frame at Sa = 2.30g

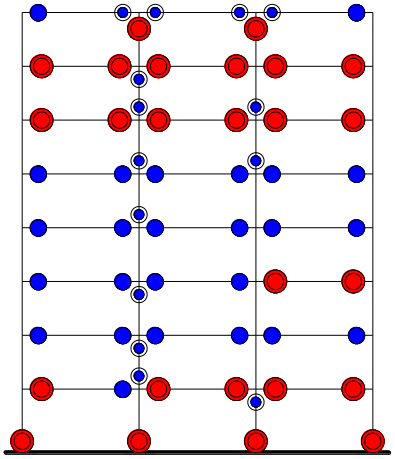

(b) The damage diagram of rocking truss-steel frame at $S_a$ = 2.30g

Fig. 12 The damage evolution process of steel frame structure and rocking truss-steel frame system under ground motion GM2

### *5.2 Structural self-resilient performance evaluation*

As shown in Figure 14, in the case of rare earthquakes, the residual deformation of the top story of the steel frame is

reduced from 9.93mm to 1.24mm, which decreases by 87.5% after adding rocking truss. When considering of the mean plus one standard deviation, the residual deformation of the top story of the steel frame is reduced from 22.70mm to 2.65mm, which decreases by 88.3% after adding rocking truss. The average residual drift angle of the second story of the structural system decreased from 0.064% to 0.007%, which was reduced by 89.1% due to the rocking truss. Residual deformation of structure will amplify second-order effect which leads to large structural damage and collapse probability, and the maintenance cost of the damaged structure will be increased. The residual deformation of steel frame can be visibly reduced when using rocking truss, thereby the repair cost will be reduced and the structural resilience under earthquakes will be improved.

### *5.3 Hysteretic performance Analysis of Self-Centering Energy Dissipative (SCED)*

The Self-Centering Energy Dissipative (SCED) is designed according to the following principles: remaining elastic under frequent earthquake; yielding to dissipate energy under fortification earthquake, and no collapse under rare earthquake. From the structural analysis under four representative ground motions (GM2, GM3, GM4, GM5), the relationships of forces and deformations of SCEDs members in rocking truss under frequent, fortification and rare earthquakes are recorded. The hysteretic curves of SCEDs under four ground motions are plotted in Figure 15. The hysteretic curve of SCED is linear under frequent earthquake, which indicates that the SCED member remains elastic without yielding, and the elastic restoring force reserved by the member can quickly restore the rocking truss-steel frame to its initial position. Compared with the steel frame, the steel frame with rocking truss shows a strong self-centering ability.

Once SCED members yield, the friction device starts to dissipate energy, and the SCED hysteretic curve shows a symmetrical "flag type". The cumulative flag curved area represents the hysteretic energy dissipation of SCED. The more loops of the hysteretic curves exist, the larger the curved area is, and the more energy is dissipated by the structural system. It shows that the residual deformations of the SCED members are little after the earthquake, and thus it can be seen that there is no residual deformation in the main steel frame. On the contrary, there are usually large structural residual deformations due to the yield of the ordinary metal braced members.

Under the rare earthquakes, the SCED will experience more hysteretic cycles and dissipate more energy. The elongation percentage of SCED can reach 1.3%, that is, the maximum elongation is 50.7mm. It can be seen that the SCED component can fully meet the performance goals.

Table 5 The damage evaluation of the steel frame and corresponding drift ratio

| Performance Level | Damage State | Drift Ratio (%) |
|---|---|---|
| I | None | $\Delta < 0.2$ |
| II | Slight | $0.2 < \Delta < 0.5$ |
| III | Light | $0.5 < \Delta < 0.7$ |
| IV | Moderate | $0.7 < \Delta < 1.5$ |
| V | Heavy | $1.5 < \Delta < 2.5$ |
| VI | Major | $2.5 < \Delta < 5.0$ |
| VII | Destroyed | $5.0 < \Delta$ |

Table 6 The drift ratio of the third story and corresponding decrease ratio with comparison to SF and SFWRT(%)

| Earthquake | Frequent earthquake | | | Fortification earthquake | | | Rare earthquake | | |
|---|---|---|---|---|---|---|---|---|---|
| Structure | SF | SFWRT | Decrease ratio | SF | SFWRT | Decrease ratio | SF | SFWRT | Decrease ratio |
| $\mu$ | 0.17 | 0.12 | 29.4 | 0.53 | 0.38 | 28.3 | 0.94 | 0.69 | 26.6 |
| $\mu+\sigma$ | 0.26 | 0.17 | 34.0 | 0.82 | 0.57 | 30.5 | 1.39 | 1.02 | 26.6 |

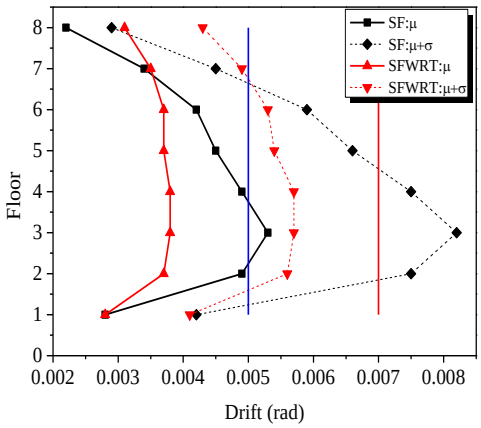


(a) Fortification earthquake

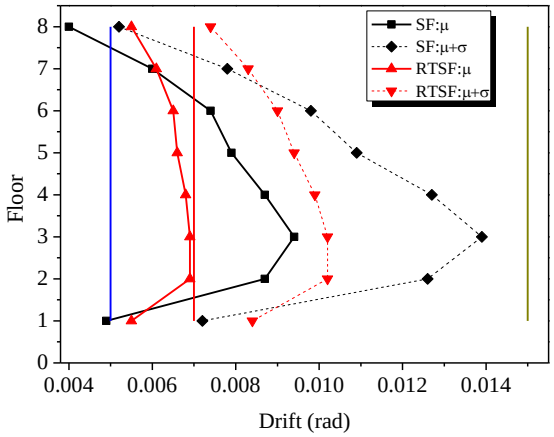


(b) Rare earthquake

Fig. 13 The drift ratios of SF and SFWRT under three earthquake intensities

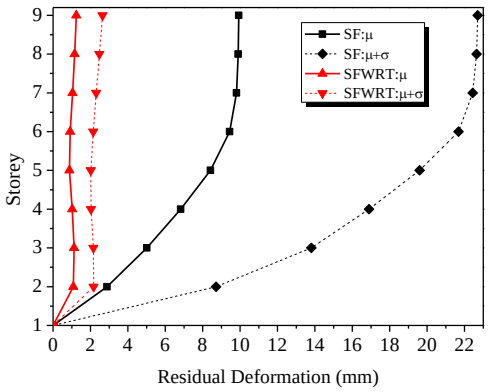


(a) Residual deformation curves

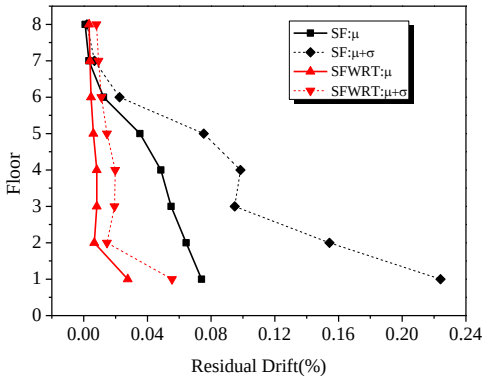


(b) Residual inter-story drift angle curves

Fig. 14 The comparison of residual deformation and residual inter-story drift angle curves

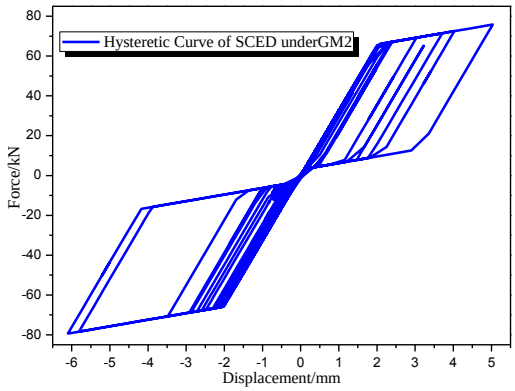


(a) Hysteretic curve of SCED under GM2

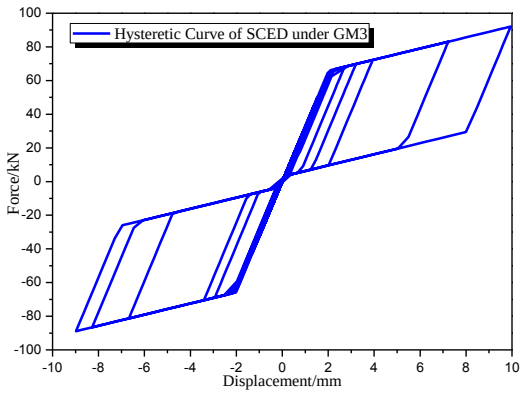


(b) Hysteretic curve of SCED under GM3

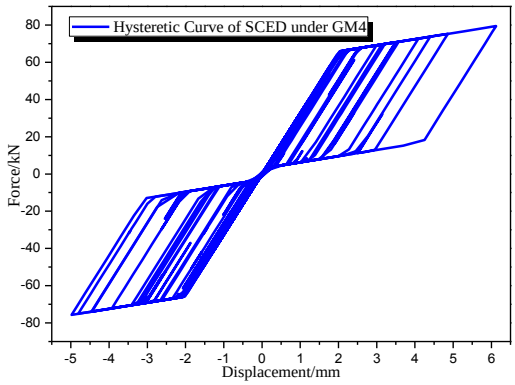


(c) Hysteretic curve of SCED under GM4

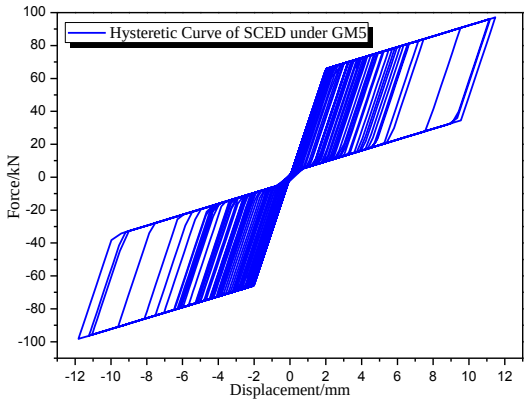


(d) Hysteretic curve of SCED under GM5

Fig. 15 SCED hysteretic curves under rare earthquake

## 6. Evaluation of structural fragility

The structural components yield successively under earthquake, which indicates the damage formation process. The selected earthquake ground motions have different intensities, duration and spectrum characteristics, so the structural damage is different under different earthquake ground motions. The structural damage evolution can be described as a process from damage appearance, damage developing and damage accumulating to failure/collapse when the damage reaches a limit state.

### *6.1 Analysis of the collapse resistance capacity*

The selected 22 earthquake records are scaled based on the structural fundamental period, whilst the Incremental Dynamic Analysis (IDA) is used to analyze/evaluate the lateral collapse resistance capacity of the models in OpenSEES. The results are depicted in the Figure 16.

A one-to-one matching relationship can be found between the IDA curve and a specified earthquake ground motion. Thus, one structural response IDA curve is also uniquely determined by each individual ground motion, and the discrepancy of the structural responses will be caused by the randomness of different ground motions. Figure 16 shows that the randomness of different ground motions has little effect on the structural response in the initial elastic stage, while the structure reaches the non-linear stage, there is a close relationship between the ground motion randomness and structural nonlinear, which is the reason why the dispersion of the responses' dispersion gradually increases.

The statistical analysis results of IDA curves under 22 ground motions of the SF and SFWRT are depicted in Figure 17, which include the 16%, 50% and 84% quantile curves. It shows that both the structures keep elastic in the initial stage when the structural deformation is small, and the ground motions have little influence on the structural responses. With the inter-story deformation increasing, the dispersion of the IDA curves is amplified, which means the large uncertainty of structural response. Moreover, the SFWRT has a smaller deformation compared to the SF, which indicates the rocking truss can significantly decrease the structural dynamic response and improve the seismic performance of the model.

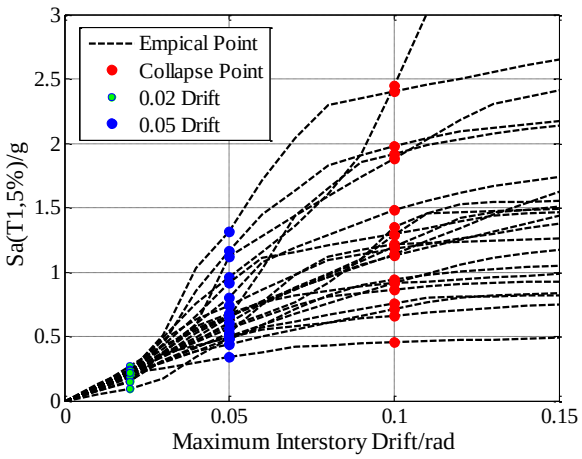


(a) the curves of steel frame

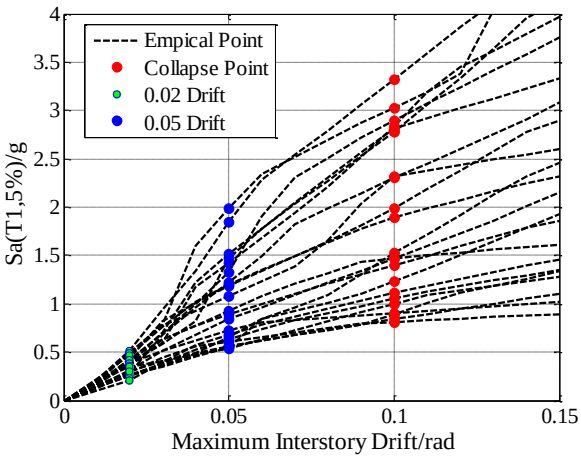


(b) the curves of steel frame with rocking truss

Fig. 16 The IDA curves of the SF and SFWRT under 22 ground motions

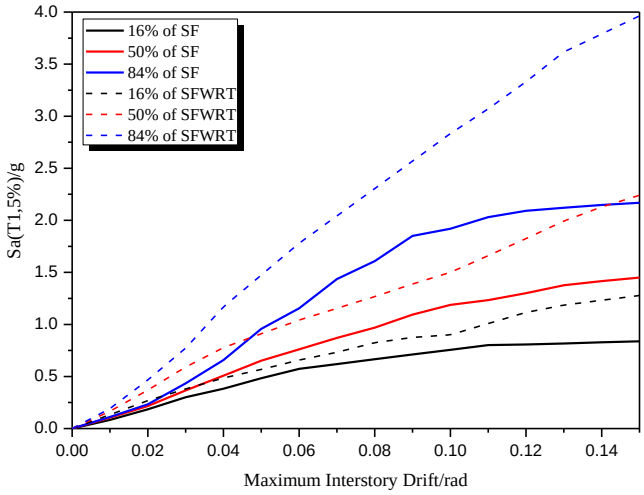


Fig. 17 The 16-percentile, 50- percentile and 84- percentile IDA curves of two structures

*6.2 Assessment of collapse probability*

Three limit states are adopted in this section to assess the structural seismic performance of the models.

Limit State 1: The new edition of Chinese Code for Seismic Design of Buildings recommends that the performance level for the steel frame structures is defined as maximum inter-story drift limited to 2.0% under rare earthquake, which is chosen as the limit state 1.

Limit State 2: As recommended by FEMA273 (1997), the collapse limit should be less than 5% story drift, which is adopted for the limit state 2 for the example structure.

Limit State 3: The FEMA350 (2000) proposed that the frame collapse intensity is defined as the smaller one of the intensity at which the slope of IDA curve is very small (i.e. the flat-line region) and the intensity corresponding to the 10% inter-story drift (beyond which the gravity framing is assumed to lose its gravity load bearing ability).

Fragility curves of collapse probability are derived based on the statistics of collapse point and a lognormal fitting for SF and SFWRT with considering the three limit states, as shown in Figure 18. The results show that the collapse probability curves corresponding to the SF and SFWRT at the limit state 3 are below the curves corresponding to limit state 2, which is also under the curves corresponding to limit state 1. Simultaneously, all the collapse probability curves of the SFWRT locate below those of SF, which indicates the contribution of rocking truss to reduce the collapse probability under earthquakes.

It is meaningful to determine the mean global collapse resistance capacity based on the ground motion intensity *Sa*(T1)50% corresponding to the collapse probability ( P[Collapse] ) is 50%, then the Collapse Margin Ratio (CMR, defined as the ratio of the practical collapse resistant capacity to the fortification seismic demand) can be calculated as follows:

$$CMR = S_a(\mathrm{T}_1)_{50\%} / S_a(\mathrm{T}_1)_{rare} \tag{4}$$

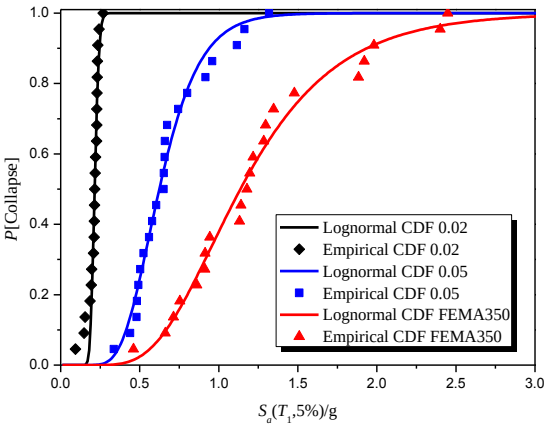


(a) The collapse probability of the SF

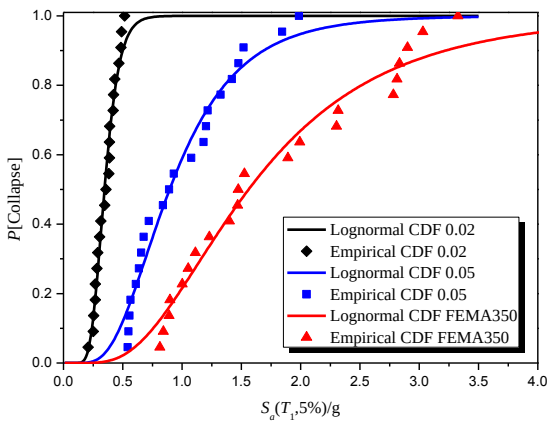


(b) The collapse probability of the SFWRT

Fig. 18 The schematic of collapse probabilities between the SF and SFWRT

where the Sa(T1)50% represents the earthquake intensity corresponding to 50% collapse probability, and the *S*a(T1)rare is the spectrum acceleration corresponding to structural fundamental period under rare earthquake level.

The Collapse Resistance Improved Index (CRII) and the Change Rate of Structural Collapse Probability (CRII=1) are also proposed to consider the improvement of structural performance, which could be calculated using Equations (5) and (6) in the rare earthquake level:

$$CRII = \frac{CM_{\mathrm{SFWRT}} - CM_{\mathrm{SF}}}{CM_{\mathrm{SF}}} \times 100\% \tag{5}$$

$$\delta_P = \left| \frac{P\left(Collapse_{\mathrm{SFWRT}} \mid S_a\left(T_1\right)_{\mathrm{rare}}\right) - P\left(Collapse_{\mathrm{SF}} \mid S_a\left(T_1\right)_{\mathrm{rare}}\right)}{P\left(Collapse_{\mathrm{SF}} \mid S_a\left(T_1\right)_{\mathrm{rare}}\right)} \right| \tag{6}$$

where *CRII* = Collapse Resistance Improved Index; $CMR_{\mathrm{SFWRT}}$ = Collapse Margin Ration of the SFWRT; $CMR_{\mathrm{SF}}$ = Collapse Margin Ration of the SF. represents the Change Rate of the Structural Collapse Probability, P($Collapse_{\mathrm{SFWRT}}$| $Sa(T1)_{\mathrm{rare}}$) and P($Collapse_{\mathrm{SF}}$|$Sa(T1)_{\mathrm{rare}}$) are the collapse probability of the SFWRT and SF under the rare earthquake level, respectively.

Based on the above definitions, the rocking truss's contributions to reduce the collapse probability are calculated using Equations (5) and (6), which are listed in Table 7 and 8. The comparisons show that the structural collapse resistance capacity has been greatly improved with the rocking truss. The collapse resistance is improved by 62.7%, and 42.9%, 37.7% under the limit state 1, 2 and 3, respectively. Besides, the structural collapse probability under the rare earthquakes can be obtained when the collapse margin ratio equals to 1. Table 8 give the probability change rate under the rare earthquake, and the SFWRT has a minimum collapse probability of 2.4% for limit state 1 when subjected to the rare earthquake. Additionally, the FEMA P695 (2009) recommends that the collapse probability of newly-built structure is below 10% under the maximum considered earthquakes (MCE), therefore the collapse probability of the SFWRT is acceptable.

Table 7 *CRII*-based collapse resistance capacity evaluation of the of the SF and SFWRT

| Limit state | 1 | 2 | 3 |
|---|---|---|---|
| SF | 1.044 | 3.058 | 5.534 |
| SFWRT | 1.699 | 4.369 | 7.621 |
| *CRII* | 62.7% | 42.9% | 37.7% |

Table 8 Change rate of the structural collapse probability under the rare earthquake (Limit State 1)

| SF | SFWRT | $\delta_P$ |
|---|---|---|
| 24.4% | 4.1% | 83.2% |

### *6.3 Comparison of structural fragility*

For the middle-rise steel moment frame, slight damage state, moderate damage state, extensive damage state and completely damage state are defined by the HAZUS (2003), and the structural fragility analysis and Structural Performance Improved Index (SPII) are implemented to discuss the contribution of the rocking truss. Especially, the SPII is defined:

$$SPII = \frac{S_{a,SFWRT} - S_{a,SF}}{S_{a,SF}} \times 100\% \tag{7}$$

where *SPII* is the structural performance improved index, and $S_{a,SFWR}$ and $S_{a,SF}$ represent the earthquake intensities when the failure probability of SFWRT and SF is 50% under different damage states, respectively.

The corresponding fragility curves and SPIIs are given in Figure 19 and Table 9. It is observed that the failure probability of the SFWRT in different limit states are smaller than that of the SF whilst that of the SPIIs in slight damage, moderate damage and extensive damage are improved by more than 50%, while the collapse resistance capacity is increased by 35.1%. Therefore, the damage of the SF as well as the expected loss of the main structure under earthquake can be significantly reduced by using rock truss.

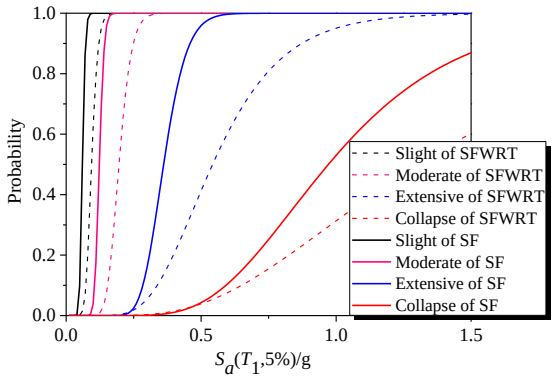


Fig. 19 The fragility curves for four limit states between SF and SFWRT

Table 9 Comparison of the seismic capacity medium value as *Sa* in different damage states (g)

| Damage state | Slight | Moderate | Extensive | Collapse |
|---|---|---|---|---|
| SF | 0.060 | 0.123 | 0.360 | 0.970 |
| SFWRT | 0.094 | 0.196 | 0.540 | 1.310 |
| *SPII* | 56.7% | 59.3% | 50.0% | 35.1% |

## 7. Conclusions

This study focuses on the collapse probability and structural fragility of an 8-story SF with and without using rocking truss, whose structural damage evolution is also discussed. The conclusions are summarized as follows:

- The addition of rocking truss in steel frame leads the plastic hinges distributed in the structural components more uniformly, compared with the steel frame without rocking truss. The failure mode can be transformed from the multi-storey failure to the expected uniform inter-story deformation and the soft story failure mode.
- IDA is used to analysis the collapse probability and fragility of SF and SFWRT, and different limit states are considered. The results show that the collapse probability and failure probability of SFWRT are obviously lower than those of SF, which indicates that the rocking truss can significantly improve the seismic performance and the structural resilience of the SF.
- The statistical analysis of the failure paths is also proposed to validate the efficiency of assembling rocking truss. It concludes that the local damage concentration is always observed for SF, which leads to a soft story and the collapse would be caused by the intensified local damage. On the contrary, SFWRT shows a more uniform structural damage and better global performance. The failure path of SFWRT is also more reasonable, compared with SF under the earthquake.

## Acknowledgments

The research described in this paper was financially supported by National Natural Science Foundation of China (51978220, 51908085), Scientific Research Fund of Institute of Engineering Mechanics, China Earthquake Administration (2018D04), National Key Research and Development Program Project (2019YFE0112400), Natural Science Foundation of Chongqing (cstc2020jcyj-msxmX0010), Fundamental Research Funds for the Central Universities (2020CDJ-LHZZ-013).

## References

Blebo F C, Roke D A. (2018), ″Seismic-resistant self-centering rocking core system with buckling restrained columns″. Engineering Structures, 173: 372-382.

Chopra A K, Goel R K. (2014), ″Building period formulas for estimating seismic displacements″. Earthquake Spectra, 16(2): 533-536.

Christopoulos C, Tremblay R, Kim H J, et al. (2008), Self-Centering energy dissipative bracing system for the seismic resistance of structures: development and validation. Structural Engineering, 134(1): 96-107.

Clough, R.W., and Huckelbridge, A. A. (1977), “Preliminary experimental study of seismic uplift of a steel frame”. Report No.

UCB/EERC-77-22, Earthquake Engineering Research Center (EERC), University of California, Berkeley, CA.

Dar A, Konstantinidis D, El-Dakhakhni W. (2018), ″Seismic response of rocking frames with top support eccentricity″. Earthquake Engineering & Structural Dynamics, 47(12): 2496-2518.

Deierlein G, Krawinkler H, Ma X, et al. (2011), "Earthquake resilient steel braced frames with controlled rocking and energy dissipating fuses". Steel Construction, 4(3): 171-175.

Du Y.F, Wu D.Y. (2014), "Performance analysis of light energy dissipative rocking frame designed on the basis of stiffness demand". China Civil Engineering Journal, 47(1): 25-35.

Eatherton M R, Hajjar J F, Deierlein G G. (2008), "Controlled rocking of steel-framed buildings with replaceable energy-dissipating fuses",. The 14th World Conference on Earthquake Engineering, Beijing, China, October.

Federal Emergency Management Agency. (2003), "Multi-hazard loss estimation methodology. Earthquake model". Washington, DC: HAZUS-MH MR1 Technical Manual.

FEMA-350. (2000), "Recommended seismic design criteria for new steel moment-frame buildings". Federal Emergency Management Agency: Washington, D.C.

FEMA-273. (1997), "NEHPR Guidelines for the seismic rehabilitation of building". Federal Emergency Management Agency: Washington, D.C.

FEMA-695. (2009), "Quantification of building seismic performance factors". Federal Emergency Management Agency: Washington, D.C.

GB50011-2010. (2010), "Code for seismic design of buildings". Beijing: National Standards of the People's Republic of China, China Architecture & Building Press. (in Chinese)

Gledhill, S. M., Sidwell, G. K., and Bell, D. K. (2008), "The damage avoidance design of tall steel frame buildings-Fairlie terrace student accommodation project", Victoria University of Wellington. New Zealand Society for Earthquake Engineering Conf., New Zealand Society for Earthquake Engineering, Wellington, New Zealand.

Gunay S, Korolyk D, Mar D, Mosalam K, Rodgers J. (2009), "Infill walls as a spine to enhance the seismic performance of non-ductile reinforced concrete frames". ATC & SEI conference on improving the seismic performance of existing buildings and other structures, ASCE; December.

Hall, K S, Eatherton M. (2010), and Hajjar, J. F. "Nonlinear behavior of controlled rocking steel-framed building systems with replaceable energy dissipating fuses". Report No. NSEL-026, Newmark Structural Engineering Laboratory Report Series, Urbana, IL.

Jia L, Li R, Xiang P, et al. (2018), ″Resilient steel frames installed with self-centering dual-steel buckling-restrained brace″. Journal of Constructional Steel Research, 149: 95-104.

Jia M, Gao S, Lu D G, et al. (2019) Collapse resistance assessment of buckling-restrained braced steel frames using combined deterministic and probability analysis approach. International Journal of Earthquake Engineering. 3: 31-51.

Kamperidis V C, Karavasilis T L, Vasdravellis G. (2018), ″Self-centering steel column base with metallic energy dissipation devices″. Journal of Constructional Steel Research, 2018, 149: 14-30.

Keivan A, Zhang Y. (2019), ″Nonlinear seismic performance of Y-type self-centering steel eccentrically braced frame buildings″. Engineering Structures, 179: 448-459.

Kibriya L T, Málaga-Chuquitaype C, Kashani M M, et al. (2018), ″Nonlinear dynamics of self-centering rocking steel frames using finite element models″. Soil Dynamics and Earthquake Engineering, 115: 826-837.

MacRae G A, Kimura Y, Roeder C. (2004), "Effect of column stiffness on braced frame seismic behavior". Journal of Structural Engineering, (3): 381-391.

Matthew R. Eatherton, M. ASCE, Xiang Ma, A.M. ASCE, Helmut Krawinkler, M.ASCE et al. (2014), "Design concepts for controlled rocking of self-centering steel-braced frames". Journal of Structural Engineering, 140(11):04014082.

Michael Pollino. (2015), "Seismic design for enhanced building performance using rocking steel braced frames". Engineering Structures,

83: 129-139.

Midorikawa M, Azuhata T, Ishihara T. (2002), “Earthquake response reduction of buildings by rocking structural systems”. Smart Structures and Materials: 265-272.

Midorikawa M, Azuhata T, Ishihara T. (2014), “Shaking table tests on seismic response of steel braced frames with column uplift”. Earthquake Engineering & Structural Dynamics, 35(14): 1767-1785.

Pollino M, Sabzehzar S, Qu B, Mosqueda G. (2013), “Research needs for seismic rehabilitation of sub-standard buildings using stiff rocking cores”. ASCE Structures Congress, Pittsburgh, PA; May.

Qu Z. (2010), “Study on seismic damage mechanism control and design of rocking wall-frame structures”. Tsinghua University Department of Civil Engineering,

Qu Z, Wada A, Ye L.P. (2011), “Seismic retrofit of frame structures using rocking wall system”. Journal of Building Structures, 32(9): 11-19.

Tremblay, R., et al. (2008), “Innovative viscously damped rocking braced steel frames”. 14th World Conf. on Earthquake Engineering, Beijing, China.

Vassiliou M F, Mackie K R, Stojadinović B. (2017), “A finite element model for seismic response analysis of deformable rocking frames”. Earthquake Engineering & Structural Dynamics, 46(3): 447-466.

Wada A, Qu Z, Ito H. (2009), “Seismic retrofit using rocking walls and steel dampers”. ATC/SEI Conference on Improving the Seismic Performance of Existing Building and Other Structures, San Francisco, CA, U.S.

Wen Y K, Kang Y J. (2009), “Minimum building life-cycle cost design”, Ⅰ: Methodology and Ⅱ: Application.

Wu D.Y. (2013), “Seismic mitigation of an innovative light energy dissipative rocking frame under near-field ground motions”. Lanzhou University of Technology Collage of Civil Engineering, (in Chinese)

Zhang G, Chen P, Zhao Z, et al. (2018), “Experimental study on seismic performance of rocking buckling-restrained brace steel frame with liftable column base”. Journal of Constructional Steel Research, 143: 291-306.